Improving the finite element model accuracy of tissue engineered scaffolds produced by selective laser sintering

The original publication was published in the Journal of Materials Science Materials in Medicine (2015) 26: 38.
The final publication is available at Springer via http://dx.doi.org/10.1007/s10856-014-5376-0

Improving the Finite Element Model Accuracy of Tissue Engineering Scaffolds Produced by Selective Laser Sintering

S. Lohfeld, S. Cahill, H. Doyle, P.E. McHugh

Biomechanics Research Centre (BMEC), Mechanical and Biomedical Engineering, College of Engineering and Informatics, National University of Ireland Galway, Galway, Ireland

Abstract

In bone tissue engineering, both geometrical and mechanical properties of a scaffold play a major part in the success the treatment. The mechanical stresses and strains that act on cells on a scaffold in a physiological environment are a determining factor on the subsequent tissue formation. Computational models are often used to simulate the effect of changes of internal architectures and external loads applied to the scaffold in order to optimise the scaffold geometry for the prospective implantation site. Finite element analysis (FEA) based on computer models of the scaffold is a common technique, but would not take into account actual inaccuracies due to the manufacturing process. Image based FEA using CT scans of fabricated scaffolds can provide a more accurate analysis of the scaffold, and was used in this work in order to accurately simulate and predict the mechanical performance of bone tissue engineering scaffolds, fabricated using selective laser sintering (SLS), with a view to generating a methodology that could be used to optimise scaffold design. The present work revealed that an approach that assumes isotropic properties of SLS fabricated scaffolds will lead to inaccurate predictions of the FE model. However, a dependency of the greyvalue of the CT scans and the mechanical properties was discovered, which may ultimately lead to accurate FE models without the need of experimental validation.

1 Introduction

Tissue engineering was defined by Langer and Vacanti as “an interdisciplinary field that applies the principles of engineering and life sciences toward the development of biological substitutes that restore, maintain, or improve tissue function or a whole organ” [1]. Bone tissue engineering aims to create the next generation of bone substitutes. The need for bone substitutes can arise due to trauma, disease or tumours, causing defects in the bone structure. These defects can occur anywhere in the skeleton and can vary in size, shape and severity. The main function of a bone substitute is to provide structural support to the surrounding tissue, but, ideally, a bone substitute should perform all the functions that healthy bone at the site of the defect would perform. This substitute usually is an open cellular structure known as a scaffold, with or without cells seeded prior to implantation. If biodegradable, the scaffold must perform the same mechanical functions as healthy bone in that situation only temporarily. It degrades over time and is replaced by the newly formed bone tissue grown into it, which resumes the scaffold’s functions and ideally restores the original functionality.

Both the geometrical and the mechanical properties of a scaffold play a major part in the success of a bone tissue engineering treatment. Geometrically, besides a good fit for the defect the scaffold (external architecture), the scaffold needs sufficient porosity and pore interconnectivity (internal architecture) to allow for cell growth and communication. Mechanically, not only the structural support to the surrounding tissue is important, but also the cells must receive the correct mechanical stimulus for bone formation. When a scaffold with cells is placed in vivo or into a physiological environment, the mechanical stresses and strains the cells experience are a determining factor on the subsequent tissue formation [2-8]. These stresses and strains are determined by the mechanical properties of the scaffold, by the mechanical loads placed on the scaffold, and by the manner in which fluid flows through the scaffold. As mechanical loads on a scaffold will vary from site to site, the mechanical properties of, and fluid flow through, the scaffold should be ideally adjusted for each site. This can be achieved by varying the scaffold's internal architecture, which also influences the structural support that a scaffold provides [9], and its ability to satisfy the geometrical requirements placed on the scaffolds such as porosity, pore size, and pore interconnectivity. Therefore, the internal architecture of a scaffold is a major determinant in the success of bone tissue engineering treatment. Mechanical tests can be used to examine the structural support different internal architectures provide. However, the in vivo loading conditions a scaffold will experience can be very complex, and ex vivo reproduction of these conditions is difficult. A validated computational model would ease the task. It would further allow a comparison of the stresses and strains cells seeded on scaffolds with different internal architectures experience under mechanical load.

Currently, finite element analysis (FEA) of bone scaffold mechanics in the literature is in two forms: FEA based on CAD drawings of intended designs (CAD-based FEA), and FEA based of data taken from μCT scans of fabricated scaffolds (image-based FEA). For selecting the appropriate approach, one must consider the accuracy of the fabrication method for a scaffold. Fabricating scaffolds using the powder based additive manufacturing technique "selective laser sintering" (SLS) can be challenging in terms of achieving accurate dimensions when building scaffolds that satisfy the geometrical constraints placed on them, such as size, porosity and pore size. Geometrical differences, like unintended micropores, lead to inaccurate CAD-based FEA models. High resolution image-based FEA captures the correct scaffold geometry, and hence should be more accurate. However, most reports in the literature assume isotropic material properties, which may not be correct. In μCT scans of bone, there is a relationship between local greyvalue and local material properties; the same may be true for μCT scans of scaffolds. For this reason there is a requirement to validate image-based FE models and determine whether or not the isotropic assumption is valid.

In the present work, two sets of bone tissue engineering scaffolds were fabricated with a minimum feature size and tested in compression. The first set was made from polycaprolactone (PCL) and the second set was made from a composite of polycaprolactone/tricalcium phosphate (PCL/TCP). μCT scans of the fabricated scaffolds were utilised to develop detailed FE meshes of the fabricated scaffolds. FE simulations of compression tests were then carried out and the predictions for a scaffold's effective modulus were compared with actual results obtained from compression tests. To validate whether the assumption of isotropic material properties was correct, the μCT scans and FEA results were analysed for a possible relationship between greyvalues and local material properties.

1.1 Objectives

The work presented here used finite element analysis to attempt to accurately simulate and predict the mechanical performance of bone tissue engineering scaffolds, fabricated using selective laser sintering, with a view to generating a methodology that could be used to optimise scaffold design. Optimising scaffold design using computational modelling techniques is often linked with additive manufacturing (AM) techniques, of which SLS is one, because AM techniques give a high degree of control over the scaffold's internal architecture. This control over the scaffold's internal architecture means, in theory at least, that the AM technique will be able to fabricate a scaffold with optimised design.

1.2 Literature review

A number of studies in the literature have focused on specific uses of computational modelling in bone scaffold mechanics. Several groups have proposed a library of scaffold unit cells with known mechanical and fluid flow properties which can be assembled together to form a larger scaffold with the required heterogeneity and anisotropy of the bone they replace [9-13]. Chea et al. [10] and Wettergreen et al. [9] explained how such a library would work, and the latter also demonstrated how FE analysis could be used to compare the effective modulus and stress distributions of different scaffold designs. However, the studies were lacking a validation of the CAD-based models (i.e. a model that was based on CAD drawings) by comparing computational predictions with experimental results. The majority of scaffold FE analyses in the literature to date are limited to predicting a scaffold's effective modulus and stress distribution. Studies by Luxner et al. [11], Williams et al. [14] and Eshraghi and Das [15] on FE predictions for effective modulus of bone tissue engineering scaffolds compared the results with actual compression tests. In all cases selective laser sintering was used to fabricate the scaffolds. Luxner et al. [11] found FE predictions to be accurate for scaffold designs with isotropic mechanical properties but inaccurate for scaffold designs with anisotropic properties. While Williams et al. [14] found their predictions to be accurate, loose powder was not removed from the scaffold when carrying out compression tests. The loose powder present in areas supposed to be void could have stiffened the scaffold. In a more recent publication, Eshraghi and Das reported good agreement of predicted and actual compressive effective modulus of PCL-HA composites, probably due to the high sample density achieved, but still showing an error of about 25% [15].

A further limitation in some of the above work was that it was based on scaled up models. However, a scaffold's requirement of high porosity and small pore size (less than 1 mm) means that scaffold features, i.e. the struts, would need to be fabricated with dimensions close to industrial SLS system's minimum feature size. It is possible that at this size scale the mechanical properties of the fabricated scaffold would have been different. In a study by Cahill et al. [16], scaffolds with the small feature size necessary for bone tissue engineering were fabricated via SLS and tested in compression. A CAD-based FE model gave the same predictions for the same scaffold designs as those of Wettergreen et al. [9] and Luxner et al. [11] and was then used to predict how the fabricated scaffolds would perform in compression tests. It was found that the FE model overpredicted the effective modulus for each material-based directional modulus being measured. The range of overprediction varied from 67 % to 147 % depending on the direction of the effective moduli being measured. It was also found that the existence and extent of continuous paths of load supporting material within the scaffold in the direction of loading, to be one of the primary factors in determining the scaffolds effective modulus in that direction. However, these CAD-based FE models did not account for topographical features in the fabricated scaffold, such as surface roughness and micropores. These geometrical features reduce the effective size of the continuous paths of load bearing material and therefore reduce the scaffold's effective modulus. Hence, the CAD-based FE models gave higher values than obtained in the experiments.

Other groups have shown the potential of image-based FEA, i.e. FE analysis using data obtained from μCT scans, for predicting scaffold stress distributions and for demonstrating where stress concentrations are likely to occur [14, 17-20]. However, again experimental validation of these results has not been reported.

2 Methods

Scaffold fabrication

Two sets of scaffolds were fabricated via SLS. All scaffolds were manufactured using a DTM Sinterstation 2500^{plus} (DTM, Houston, Texas, USA). The first set of scaffolds was fabricated from polycaprolactone powder ("PCL", CAPA 6506, Solvay Caprolactones, UK), while for the second set a composite powder consisting of 90 % PCL and 10 % β-tri-calcium phosphate ("TCP", Fluka, Sigma-Aldrich Chemie GmbH, Germany) was processed. The scaffolds were fabricated using the "outline scan" function as described elsewhere [16, 21].

The PCL scaffolds and four of the PCL/TCP scaffolds consisted of layers of parallel struts, the orientations of which were changed from layer to layer. To improve stiffness, two of the PCL scaffolds were encircled by a porous cage. The PCL scaffold designs P1 to P4 are listed in Table 1. Four of the PCL/TCP designs (PT1 to PT4) were similar to the PCL scaffold layout (see Table 2), while two more PCL/TCP scaffolds listed in Table 3 (PT5 and PT6) consisted of repeating unit cells that could be used in a library and should give the tissue engineer greater control over the mechanical properties. The unit cells chosen were those recommended by Luxner et al. [11].

Mechanical testing

All scaffolds were mechanically tested under compression, and Vernier callipers were used to measure scaffold dimensions. The PCL scaffolds were tested on a material testing machine (Z2.5, Zwick, Ulm, Germany) using a 1 kN load cell and at a compression rate of 5 mm/min. The load applied was measured using the load cell, while the strain was measured based on grip separation. Compression tests on the PCL/TCP scaffolds were carried out using a universal testing machine (Z010, Zwick, Ulm, Germany). The test set-up for all the PCL/TCP samples is shown in Fig. 1. The height of the sample was taken as the height at which the testing machine reached its preload. The load was again applied at a rate of 5 mm/min. To measure axial displacement, and hence determine strain, a displacement transducer was used. The transducer has an accuracy of ±1 μm. For each scaffold type, a minimum of eight samples were tested.

μCT scans

μCT scans of all scaffolds were taken on Skyscan 1072 μCT scanning systems (Skyscan, Belgium). The PCL scaffolds were scanned with a resolution of 11.1 μm at the University of Naples, Italy, while the PCL/TCP scaffolds were scanned with a resolution of 10.1 μm at University of Aberdeen, UK. The scaffolds were compared only within their groups, hence the difference in calibration of the two scanners should not have influenced the results presented here.

FE mesh creation

As the resolution of the μCT scanner was too low, it could not pick up the TCP particles (size 3-5 μm). Therefore, they were not included in the FE models for the PCL/TCP scaffolds. To account for the missing μCT scans slices at the top and bottom of the scaffolds, sufficient bitmap images of the existing top and bottom layers were duplicated and added in to correct the thickness in these regions. To reduce computational workload, the resolution of the bitmap images was lowered by a factor of three. The resulting bitmap images were then converted into

3D finite element meshes using a voxel mesher developed by Harrison et al. [22]. The greyvalue scale in the voxel mesher was set linearly with 0 representing black and 1 representing white. The voxel mesher separated the pixels which formed the scaffold from the background using a threshold of 0.2 and used them to form a 3D mesh. When the 3D mesh was created, elements which were not joined to the main 3D structure were removed because the pixels that were used to form these elements were assumed to be background noise.

The created meshes consisted of 8-noded linear elements with length, width, and height equal to the resolution of the bitmap images used to create the mesh (33.3 μm for the PCL scaffolds and 30.3 μm for the PCL/TCP scaffolds). All the elements were smaller than the smallest PCL particles, which had a diameter range of 50-110 μm. The detail of the meshes is shown in the example in Fig. 2. For the PCL/TCP scaffold models, a layer of solid material was added to each end to represent the compression plates in order to facilitate applying the boundary conditions in the FE analysis.

FE analysis

The FE analysis was performed using ABAQUS v6.5 (DS Simulia, USA). To simulate compression tests, all nodes bar one at the bottom end of the scaffold were constrained in the direction of loading and the remaining node was constrained in all three directions. At the top end of the scaffold, all nodes were coupled and were given a displacement corresponding to a compressive strain of 1 %. The effective modulus of the scaffold was then calculated by inputting the resultant reaction force generated at the top end into equation 1:

$$\frac{F_R}{A_{CS}} = E_{effective}\varepsilon_A \tag{1}$$

where F_R is the reaction force, A_{CS} is the total cross-sectional area, $E_{effective}$ is the effective modulus and ε_A is the applied engineering strain.

The materials were assumed to be isotropic with a Poisson's ratio of 0.3. The initial intention was to determine the necessary elastic modulus for input to the models from compression tests on "fully solid" sintered samples. However, μCT analysis revealed that these intentionally fully solid samples actually still had an average porosity of 22 %. Therefore, reliable elastic moduli for the material at the local level could not be determined from such tests. As a result, an alternative fitting-based strategy was adopted to determine the input elastic moduli for the FE models. In this, the modulus required for an accurate prediction of the effective modulus for one scaffold design was identified in each scaffold material set (PCL and PCL/TCP, respectively), and then it was used as the input elastic modulus value for the other scaffolds in that set.

Greyvalues

Studies on μCT scans of bone and the mechanical properties of the scanned bone have shown that a correlation exists between the greyvalue of the scan at a particular point and the elastic modulus at that point. Higher greyvalues mean higher elastic moduli [22, 23]. If such a relationship exists for the scaffolds fabricated in this work, the variation in greyvalue data throughout the μCT scan of the scaffold would be evidence of variation in local material properties and powder binding strength throughout the scaffold.

To check whether a correlation between greyvalue and mechanical properties existed for the scaffolds tested, the average greyvalue of the μCT scan pixels used in creating the voxel mesh was compared with the input elastic modulus required for an accurate FE prediction of the effective modulus for that scaffold. If the required modulus was the same regardless of the average greyvalue, then there would be no such relationship. However, if for higher average greyvalues a higher or lower input elastic modulus was required, then a relationship would be present.

The average greyvalue of each scaffold was established by a MATLAB (The MathWorks Inc., USA) program which analysed the µCT images, recorded the greyvalue of every pixel used in forming the 3D mesh, and calculated the average of all greyvalues gathered.

Microporosity

While most of the work in the literature focuses on comparing intended and actual porosity [24], to the author's knowledge there are no reports of measurements of unintentional micropores or surface roughness that are present in the scaffolds. In this work, unintentional microstructural features, such as micropores resulting from the production process, were measured using MATLAB by examining images of each individual strut in all scaffolds.

SEM images

Scanning electron microscope (SEM) investigations were performed using a Hitachi S-4700 scanning electron microscope (Hitachi Scientific Instruments, Berkshire, UK) with an attached X-ray analysis system.

3 Results

Scaffold fabrication and mechanical testing

PCL scaffolds of all designs P1 through P4 were successfully fabricated in one build. For the PCL/TCP scaffolds, only the types PT1 through PT4 were fabricated in one build. PT5 and PT6 had to be produced again in a second build with reduced laser power, because the denser strut network in these unit cell designs caused excessive heat between the struts. This led to unwanted sintering and blocked pores in the first build. For the mechanical testing at least 8 samples were tested for each scaffold design.

FE analysis

By choosing an input elastic modulus that resulted in an accurate effective modulus prediction in the FE model of the P1 scaffold, the FE models for the other PCL scaffolds were run and the effective elastic modulus extracted. The experimental results and the FE predictions are given in Fig. 3. Although there is a reasonable correlation between experimental measurements and FE predictions, there is a significant discrepancy for the P4 scaffold. The same process was applied to the PCL/TCP scaffolds, identifying an input elastic modulus that gave an accurate match for the PT1 scaffold, and using this throughout the full set of scaffold models. The results of this are given in Fig. 4. A reasonable correlation between experimental measurements and FE predictions is observed for the PT1, PT2, PT3 and PT4 scaffolds, with significant discrepancies noted for the PT5 and PT6 scaffolds. In overall terms, both figures suggest that different input elastic properties are needed for each scaffold design.

Greyvalues

The average µCT greyvalue and the corresponding input elastic modulus required to generate an accurate effective modulus in the FE analysis of each PCL scaffold are given in Fig. 5. Here it can be seen that an increase in average greyvalue corresponds to an increase in required input modulus. A similar result can be observed for the PCL/TCP scaffolds in Fig. 6, with the obvious exception of the PT6 scaffold.

Microporosity measurements

All the PCL scaffolds were fabricated in the same build at the same laser power, laser scan speed, and chamber temperature. The only variants in the scaffold design were the distance between the centrelines of scaffold struts (centreline spacing) and the orientation of the scaffold struts. A study was carried out to see if there was a relationship between centreline spacing and local microporosity. It is evident from the results shown in Fig. 7 that the microporosity increases with centreline spacing.

SEM

SEM imaging, Fig. 8, showed a random distribution of the TCP particles throughout the scaffold. The TCP particles, which had a diameter of less than 5 µm, were attached to the surface of the PCL particles, all of which had a diameter greater than 50 µm.

4 Discussion

This study provides evidence that, when attempting to achieve minimum feature size, the accuracy of the SLS fabrication process is design dependent. This design dependence affects the results of the scaffold fabrication in at least two areas: 1) the elastic modulus of the powder particle bonds, and 2) the geometrical properties of the scaffold. Although all PCL scaffolds were fabricated in the same batch with the same build parameters, the required elastic modulus for accurate FE predictions was different for each scaffold design. The same was found to be true with the PCL/TCP scaffolds where four of the six scaffold designs (PT1 to PT4) were fabricated using the same parameters. For the other two scaffolds PT5 and PT6, it became necessary to adjust their design (increased strut distance) before it was possible to achieve porous constructs.

Scaffold design can influence energy applied during sintering

The scaffold design influences the energy density applied to the powder particles in two ways: 1) The design determines the centreline spacing (distance between sintering paths) and 2) certain designs require the laser to sinter certain areas twice.

When the laser beam’s centre point scans along the centreline of the CAD model strut, it sinters a strut of approximately the width of the laser beam diameter by applying energy to every point on that line. However, some of this energy dissipates to neighbouring powder particles. That means that the zone being influenced by the laser is wider than the laser beam itself. If the centreline spacing is small, then the dissipated energy from the sintering of one strut will participate in the sintering of neighbouring struts. This effect decreases with an increase in centreline spacing. In some designs, when struts cross each other, e.g. in the top and bottom layers of scaffolds P1 and P2, the crossing points are sintered twice, causing extra energy to be applied to those spots.

Relationship between energy density, geometrical properties, and greyvalues

The relationship between energy density and geometrical properties became apparent in the first sintering results of scaffolds PT5 and PT6. Here the unit cells were too small and had to be enlarged to prevent complete sintering of the structure. For a scaffold with struts close together, the energy density had to be reduced to avoid too much energy added in any given area of the scaffold. Likewise, microporosity in the struts increased with the distance between them, so the laser didn’t add additional energy into the neighbouring ones, which would have lowered the microporosity. Finally, from the µCT scans it was obvious that the density of the caged scaffolds appeared to be higher in the regions where struts and cage overlapped (Fig. 9). In these areas the scans show higher greyvalues, meaning a higher density of the structure.

Relationship between energy density, mechanical properties, and greyvalues

Similar to what is shown here, Caulfield et al. [25] found that lower energy density meant higher microporosity. Caulfield el al. used this to explain intentionally solid samples having lower elastic moduli when sintered with a lower energy density. However, in this study, the voxel-based FE meshes captured the scaffold geometry, including micropores, in high detail and would have incorporated the effects of the microporosity. The differences in elastic modulus must have been caused by differences in the powder binding strengths.

Further investigation uncovered a link between greyvalues and material properties: in general, higher greyvalues mean higher local elastic moduli (Fig. 5 and 6). This can be understood when µCT scan images are compared with SEM images. In Fig. 10a, the strut outline of the scaffold is visible. The laser scanned along the centre of each of these struts, meaning more energy was applied to the powder particles forming the centre than to those at the edges. The greyvalues are also much higher in the centre than at the edges. This is evidence of a link between them and the laser energy applied to the powder particles. In Fig. 10b, the strut centres appear smooth or fully sintered while the edges consist of loose powder particles partially attached to the scaffold structure. This suggests that particles in areas represented by higher greyvalues are more likely to be fully sintered together than in those with lower ones.

Along with the relationship of higher greyvalues and higher elastic moduli in general, this proposes that with increasing energy applied to sinter two powder particles together, the bonding strength grows, too. It also causes a greater local elastic modulus and a higher greyvalue of those particles in a µCT scan image.

However, an exception to the final statement in the last paragraph may occur in cases where greyvalues of the µCT scan image and the energy applied are above some threshold. This break of the trend, which occurred for the scaffold with the highest average greyvalue in the µCT scan (PT6), is apparent in Fig. 6. It may be explained by Caulfield's observation that above a certain value, increased energy density resulted in a decreased elastic modulus of sintered material, because material is being burned [25].

The link between partially sintered powder particles and low greyvalues in Fig. 10 also explains the connection between low greyvalues and high porosities, because a cluster of partially sintered powder particles is more porous than an area with fully sintered powder particles.

To make the FE predictions more accurate, it was attempted to correlate the input elastic modulus with the average greyvalue for each scaffold.

This correlation was carried out by taking those scaffolds in each group (PCL and PCL/TCP, respectively) with the highest and lowest average greyvalue, and matching these values with the elastic modulus required to generate an accurate FE prediction for the effective modulus for the corresponding scaffold. Linear interpolation was then used to assign elastic moduli to the remaining average greyvalues. The new correlated values were used along with a Poisson's ratio of 0.3 as isotropic input values in the voxel-based FE models.

Fig. 11 presents the predictions of this *greyvalue FE approach* for the PCL scaffolds and compares them with the experimental results and the *fitted FE approach* predictions that are presented in Fig. 3. Here, this new approach generated better accuracy than the *fitted FE approach* used previously. Fig. 12 presents equivalent data for the PCL/TCP scaffolds. In this case, in contrast, the *greyvalue FE approach* appears less accurate than the *fitted FE approach* predictions. This is probably due to a strong mismatch between the interpolated input elastic moduli and the actual required value for some scaffolds. PT6 provided the highest greyvalue and a significantly higher required E-modulus than the scaffolds PT1 through PT4. Hence, the interpolated values don't correspond well with the values shown in Fig. 6, and the FE calculation led to in extensively deviant results. However, when the unit cell based scaffolds (PT5 and PT6) are excluded from the analysis, the *greyvalue FE approach* predictions become again more accurate than the *fitted FE approach* predictions (Fig. 13), because the interpolated values are close to those depicted in Fig. 6. The scaffolds PT5 and PT6 had to be fabricated in a separate build with different build parameters and hence appear to have different properties that deteriorate the accuracy of the predictions. As discussed above, the decrease in elastic modulus of PT6, despite its high greyvalue, may be due to degradation of the material during sintering.

Still, a major limitation of the technique described above for assigning material properties to FE models is its failure to account for localised greyvalue distribution. As it was noted by Cahill et al. [16], a continuous path of material in the direction of loading plays the main role in resisting load within that scaffold. Fig. 14 shows that for the P4 scaffold. The areas with higher greyvalues (e.g. at the cage) were also those areas where continuous paths of material existed from top to bottom, i.e. there was a pixel marked white at the same position in each slice of the µCT scan throughout the height of the scaffold. This is evidence that the scaffold regions which have high greyvalues in µCT scans tend to be the regions which play a major role in resisting load.

5 Outlook

Generating accurate image-based FE models

The next challenge in generating accurate FE models is to assign material properties based on greyvalues. For this, it is necessary to establish elastic moduli that correspond to the various greyvalues. An effective technique to achieve this has been developed by Harrison et al. [22]. In their work, which was FE modelling of heterogeneous bone, nanoindentation was carried out on bone trabeculae, and a range of local elastic moduli determined. The highest and lowest elastic moduli were then matched with the highest and lowest greyvalues, and linear interpolation of elastic moduli and greyvalues carried out. Then, each element in their mesh was assigned material properties based on the greyvalue of the pixel used to create that element. The resultant FE model was found to be accurate. If an adjustment to this technique was made to accommodate for the transverse isotropy of SLS processed material, it could be used when modelling scaffolds fabricated via SLS.

Generating accurate FE models before fabrication

The ideal in computational modelling of bone tissue engineering scaffolds is to be able to predict a scaffold's performance before it is fabricated. It was shown in previous work that this was difficult because of unintended differences between actual fabricated scaffold and intended design [16]. So, in order to have accurate predictions before fabrication, the tissue engineer needs to be able to quantify the likely differences between the CAD model and the resulting scaffold.

In the present study, it was found that energy density influences the microporosity and local material properties. Therefore, in order to have accurate FE models before fabrication two things are necessary:

1) A detailed relationship which correlates different energy density values with microporosities and material properties.
2) An ability to predict the energy density applied to the different powder particles as a function of the scaffold design.

Establishing a mathematical correlation between greyvalues and the energy density would be extremely useful as 1) it could be used in conjunction with the method developed by Harrison et al. [22] to relate energy density to the material properties of a scaffold, and 2) it could be used to establish how the applied energy density varies throughout different scaffold designs.

While image-based FE analysis is more accurate as it is based on the actual manufactured scaffold shape, it has the drawback that for this type of study a scaffold must be produced. If the analysis results in the necessity of a design revision, a new scaffold needs to be produced. Several iteration steps may be necessary until the optimal scaffold design is determined, each step including a manufactured scaffold. Reliable CAD-based FE models potentially are more useful than image based FE because they would allow for customised scaffolds to be optimised in a quicker time frame. However, at the moment, CAD-based models do not seem to be reliable, at least not when SLS is the preferred fabrication method. Hence, image-based FE appears to have a better chance to be accurate, because it allows for the analysis of actual fabricated scaffolds. Eventually, the knowledge gained from the image-based FE models may be used to generate accurate FE models without the need for physical models.

6 Conclusion

The aim of this study was to develop a finite element model that captures the correct scaffold geometry of scaffolds fabricated via selective laser sintering, and to validate the FE model by comparing its predictions with results obtained from compression tests on the fabricated scaffolds. However, the validation showed that even voxel meshed models generated from μCT scans, which are a very good geometrical representation of the original scaffold, were still inaccurate. This work found that in order to achieve accurate FE predictions different material input values were needed for different scaffold designs. This result is significant because to date, to the author's knowledge, all FE models in the literature have assumed that the properties of a scaffold's material are isotropic and equal in value regardless of the scaffold design.

While trying to quantify the differences between intended and actual geometry of the scaffolds, the examination revealed only one consistency: the quantity of unintended micropores within a scaffold strut increased as the difference between strut centrelines increased. Other geometric measurements, such as the outer volume of as scaffold, appeared to be random or based on the specific scaffold design. This means that it is difficult to quantify and generalise on the differences between the geometry of the scaffolds as depicted in the CAD drawings of the intended scaffold and the geometry of the fabricated scaffold. The result is significant because many groups in the literature that cite the potential use of FE modelling in bone tissue engineering assume that geometrical properties of a scaffold will be known before fabrication. Presently this is not the case for scaffolds fabricated using Selective Laser Sintering.

The key finding of this work and in the finding of more accurate FE models, however, is the evidence for a relationship between greyvalues and the applied energy density. Further exploration of this dependency will benefit the development of more accurate FE models. Higher energy density means stiffer material properties, lower microporosity and higher greyvalues. If a mathematical correlation between greyvalues and energy density or microporosity and material properties, respectively, were to be established, this correlation might provide a mechanism for accessing how the energy density applied to the different powder particles varies throughout different scaffold designs.

In the future, the ideal will be use computational techniques to predict how a scaffold, fabricated using the SLS, performs before it is fabricated. To achieve this ideal, two requirements will be necessary:

1. A detailed relationship which correlates different energy density values with microporosities and material properties.
2. The ability to predict the energy density applied to the different powder particles as a function of scaffold design.

A detailed understanding of the relationship between greyvalue and energy density would be invaluable in achieving these two requirements.

Acknowledgements

Thanks for performing the μCT scans to the University of Naples, Italy (PCL scaffolds), and to the University of Aberdeen, UK (PCL/TCP scaffolds). The authors acknowledge research funding from the European Union through the FP6 project “STEPS” (contract number FP6-500465, www.stepsproject.com))

References

[1] Langer R, Vacanti J. Tissue engineering. Science. 1993;260:920-6.

[2] Brown TD. Techniques for mechanical stimulation of cells in vitro: a review. Journal of Biomechanics. 2000;33:3-14.

[3] Butler DL, Goldstein SA, Guilak F. Functional Tissue Engineering, the Role of Biomechanics. Journal of Biomechanical Engineering. 2000;122:570-5.

[4] Davies J. Mechanisms of endosseous integration. The International journal of prosthodontics. 1998;11:391-401.

[5] Hollister SJ, Lin CY. *Computational design of tissue engineering scaffolds*. Computer Methods in Applied Mechanics and Engineering. 2007;196:2991-8.

[6] Ikegame M, Ishibashi K, Yoshizawa T, Shimomura J, Komori T, Ozawa H, et al. Tensile Stress Induces Bone Morphogenetic Protein 4 in Preosteoblastic and Fibroblastic Cells, Which Later Differentiate into Osteoblasts Leading to Osteogenesis in the Mouse Calvariae in Organ Culture. Journal of Bone and Mineral Research. 2001;16:24-32.

[7] Lo H, Ponticiello MS, Leong KW. Fabrication of Controlled Release Biodegradable Foams by Phase Separation. Tissue Engineering. 1995;1:15-28.

[8] Mullender M, Haj AJE, Yang Y, van Duin MA, Burger EH, Klein-Nulend J. Mechanotransduction of bone cellsin vitro: Mechanobiology of bone tissue Medical and Biological Engineering and Computing. 2006;42:14-21.

[9] Wettergreen MA, Bucklen S, Starly B, Yuksel E, Sun W, Liebschner MAK. Creation of a unit block library of architectures for use in assembled scaffold engineering. Computer-Aided Design. 2005;37:1141-9.

[10] Cheah CM, Chua CK, Leong KR, Chua SW. Development of a Tissue Engineering Scaffold Structure Library for Rapid Prototyping. Part 2: Parametric Library and Assembly Program. The International Journal of Advanced Manufacturing Technology. 2003;21:302-12.

[11] Luxner M, Stampfl J, Pettermann H. Finite element modeling concepts and linear analyses of 3D regular open cell structures. Journal of Materials Science. 2005;40:5859-66.

[12] Naing MW, Chua CK, Leong KF, Wang Y. Fabrication of customised scaffolds using computer-aided design and rapid prototyping techniques. Rapid Prototyping Journal. 2005;11:249-59.

[13] Yang S, Leong K-F, Du Z, Chua C-K. The Design of Scaffolds for Use in Tissue Engineering. Part I. Traditional Factors. Tissue Engineering. 2001;7:679-89.

[14] Williams JM, Adewunmi A, Schek RM, Flanagan CL, Krebsbach PH, Feinberg SE, et al. Bone tissue engineering using polycaprolactone scaffolds fabricated via selective laser sintering. Biomaterials. 2005;26:4817-27.

[15] Eshraghi S, Das S. Micromechanical finite-element modeling and experimental characterization of the compressive mechanical properties of polycaprolactone–hydroxyapatite composite scaffolds prepared by selective laser sintering for bone tissue engineering. Acta Biomaterialia. 2012;8:3138-43.

[16] Cahill S, Lohfeld S, McHugh P. Finite element predictions compared to experimental results for the effective modulus of bone tissue engineering scaffolds fabricated by selective laser sintering. Journal of Materials Science: Materials in Medicine. 2009;20:1255-62.

[17] Jaecques SVN, Van Oosterwyck H, Muraru L, Van Cleynenbreugel T, De Smet E, Wevers M, et al. Individualised, micro CT-based finite element modelling as a tool for biomechanical analysis related to tissue engineering of bone. Biomaterials. 2004;25:1683-96.

[18] Lacroix D, Chateau A, Ginebra M-P, Planell JA. Micro-finite element models of bone tissue-engineering scaffolds. Biomaterials. 2006;27:5326-34.

[19] Sandino C, Planell JA, Lacroix D. A finite element study of mechanical stimuli in scaffolds for bone tissue engineering. Journal of Biomechanics. 2008;41:1005-14.

[20] Van Cleynenbreugel T, Schrooten J, Van Oosterwyck H, Vander Sloten J. Micro-CT-based screening of biomechanical and structural properties of bone tissue engineering scaffolds. Medical and Biological Engineering and Computing. 2006;44:517-25.

[21] Lohfeld S, Tyndyk MA, Cahill S, Flaherty N, Barron V, McHugh PE. A method to fabricate small features on scaffolds for tissue engineering via selective laser sintering. Journal of Biomedical Science and Engineering. 2010;3:138-47.

[22] Harrison NM, McDonnell PF, O'Mahoney DC, Kennedy OD, O'Brien FJ, McHugh PE. Heterogeneous linear elastic trabecular bone modelling using micro-CT attenuation data and experimentally measured heterogeneous tissue properties. Journal of Biomechanics. 2008;41:2589-96.

[23] Teo JCM, Si-Hoe KM, Keh JEL, Teoh SH. Correlation of cancellous bone microarchitectural parameters from microCT to CT number and bone mechanical properties. Materials Science and Engineering: C. 2007;27:333-9.

[24] Tuan HS, Hutmacher DW. Application of micro CT and computation modeling in bone tissue engineering. Computer-Aided Design. 2005;37:1151-61.

[25] Caulfield B, McHugh PE, Lohfeld S. Dependence of mechanical properties of polyamide components on build parameters in the SLS process. Journal of Materials Processing Technology. 2007;182:477-88.

Scaffold title	Visual	Description
P1	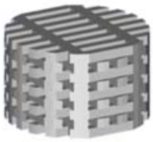	Cylindrical scaffold with diameter of 8 mm; 9 layers, each with struts orientated at 90° to the layer below
P2		Same as P1 except has a diameter of 5 mm
P3	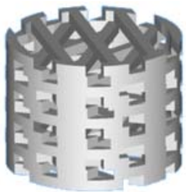	12 layers of height 0.5 mm; the struts in each layer is orientated at 30° to the struts in the previous layer. The scaffold is encircled by a porous cage.
P4	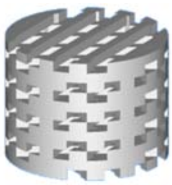	12 layers of height 0.5mm; the struts in each layer is orientated at 60° to the struts in the previous layer. The scaffold is encircled by a porous cage.

Table 1: PCL scaffolds

Scaffold title	Visual	escription
PT1	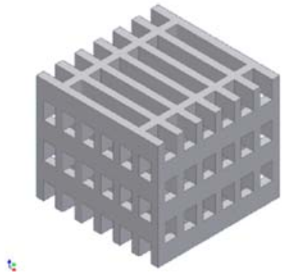	8 mm diameter, 6 layers of a height of 1 mm each; the struts in each layer are orientated at 90° to the struts in the previous layer
PT2	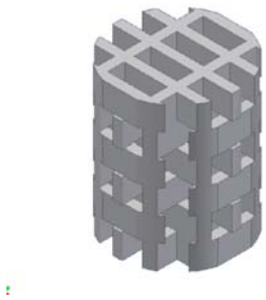	5 mm diameter, 6 layers of a height of 1 mm each; the struts in each layer are orientated at 90° to the struts in the previous layer
PT3	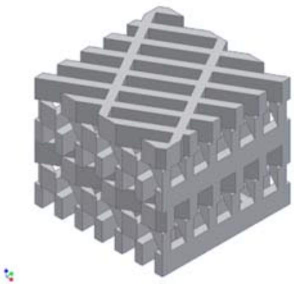	6 layers of height 1mm; the struts in each layer is orientated at 60° to the struts in the previous layer
PT4	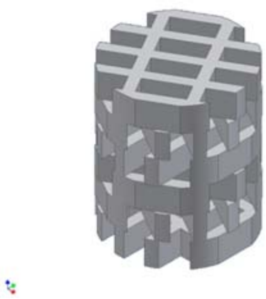	5 mm diameter, 6 layers of a height of 1 mm each; the struts in each layer is orientated at 60° to the struts in the previous layer

Table 2: PCL/TCP scaffolds

Scaffold title	Visual	Unit cell	Unit cell cut view
PT5	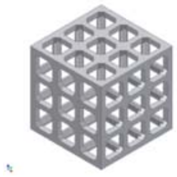 6.4 x 6.4 x 6.4 mm cube	 2 x 2 x 2 mm cube	
PT6	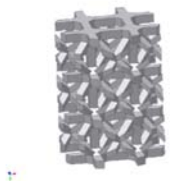 ∅ 5 mm, h = 6.4 mm	 2 x 2 x 2 mm cube	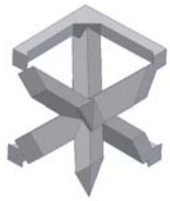

Table 3: PCL/TCP scaffolds with unit cells

Figure captions

Fig. 1: Compression test set up for smaller samples. The displacement transducer was used to measure strain.

Fig. 2: a) voxel mesh of the PT2; b) close up of part a)

Fig. 3: Experimental results compared with FE predictions for PCL scaffolds. The elastic modulus used in the FE models was such that the model gave the correct prediction for the scaffold P1. Note: for visualisation purposes, the values for the scaffold P3 are scaled up by one order of magnitude (x10).

Fig. 4: FE predictions compared with experimental results for PCL/TCP scaffolds. The elastic modulus used in the FE models was such that the model gave the correct prediction for the PT1 scaffold.

Fig. 5: Required input moduli versus average greyvalue for PCL scaffolds. This graph suggests that higher greyvalues equate with stiffer material properties.

Fig. 6: Required input moduli versus average greyvalue for PCL/TCP scaffolds. This graph suggests that higher greyvalues equate with stiffer material properties.

Fig. 7: Strut porosity vs. centreline spacing.

Fig. 8: SEM images of the PCL/TCP scaffolds. The TCP powder particles were much smaller than the PCL powder particles.

Fig. 9: The area with high greyvalues had lower porosity than the areas with low greyvalue.

Fig. 10: a) µCT scan images show struts have higher greyvalues along their centrelines than along their edges. b) SEM image shows strut has smooth surface along its centre. This is because the powder particles are fully sintered here. At the edges surface is rough, powder particles are only partially sintered.

Fig. 11: A comparison of the *greyvalue FE approach* predictions, *fitted FE approach* predictions and experimental results from compression tests for the PCL scaffolds. The *greyvalue FE approach* predictions are closer to the experimental values than the *fitted FE approach* ones. Note: as in Fig. 3, the values for the scaffold P3 are scaled up by one order of magnitude (x10) for visualisation purposes.

Fig. 12: A comparison of *greyvalue FE approach* predictions, *fitted FE approach* and experimental results from compression tests for the PCL/TCP scaffolds. The *greyvalue FE approach* predictions are less accurate than the *fitted FE approach* predictions.

Fig. 13: A comparison of *greyvalue FE approach* predictions, *fitted FE approach* predictions and experimental results from compression tests for the PCL/TCP scaffolds. In this case data from PT5 and PT6 (unit cell based scaffolds) was ignored for the *greyvalue FE approach*, and the *greyvalue FE approach* predictions are closer to the compression test results than the *fitted FE approach* predictions.

Fig. 14: a) µCT scan image of the P4 scaffold. b) Areas in this scaffold where continuous paths of material ran from top to bottom. The continuous paths are located in the areas of high greyvalues in (a).

Fig. 1: Compression test set up for smaller samples. The displacement transducer was used to measure strain.

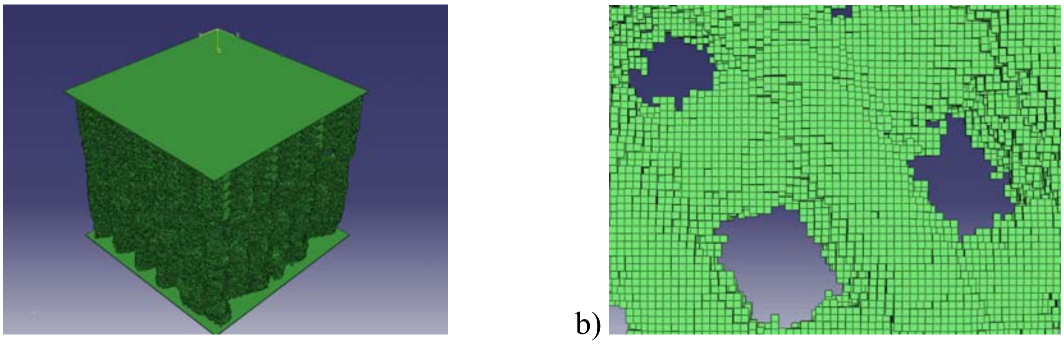

a) b)

Fig. 2: a) voxel mesh of PT2; b) close up of part a)

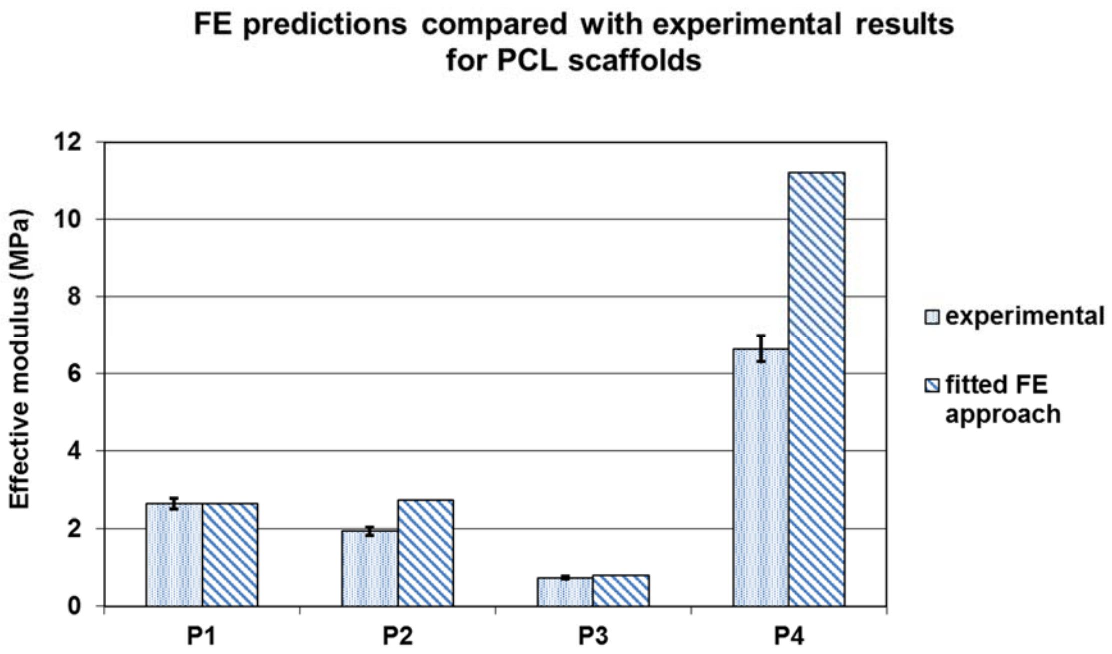

Fig. 3: Experimental results compared with FE predictions for PCL scaffolds. The elastic modulus used in the FE models was such that the model gave the correct prediction for the scaffold P1. Note: for visualisation purposes, the values for the scaffold P3 are scaled up by one order of magnitude (x10).

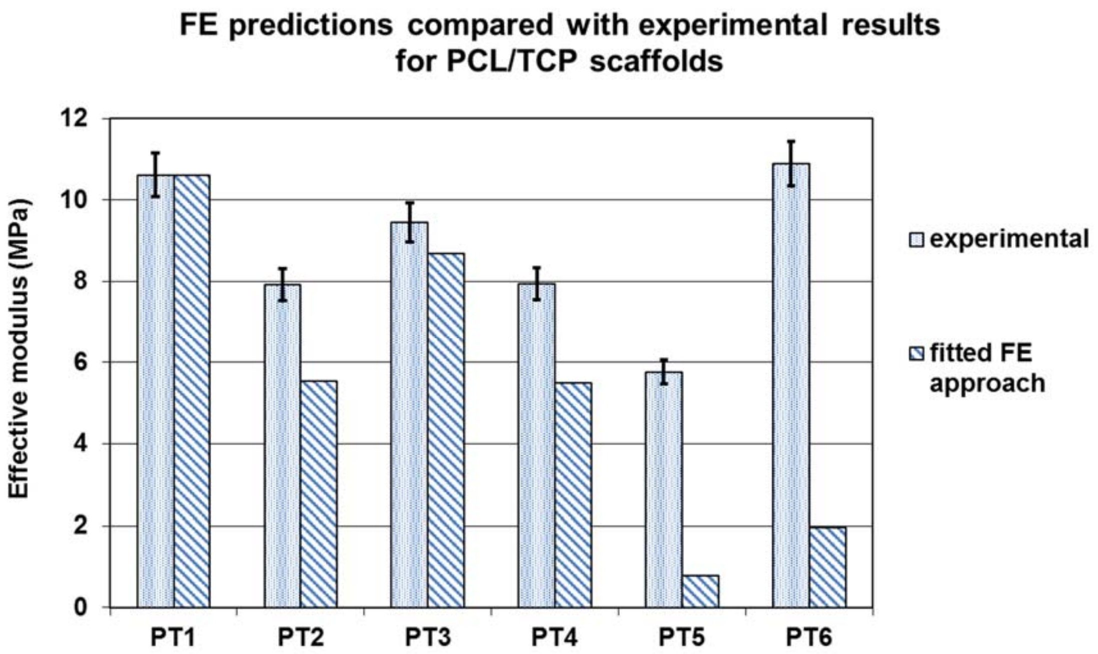

Fig. 4: FE predictions compared with experimental results for PCL/TCP scaffolds. The elastic modulus used in the FE models was such that the model gave the correct prediction for the PT1 scaffold.

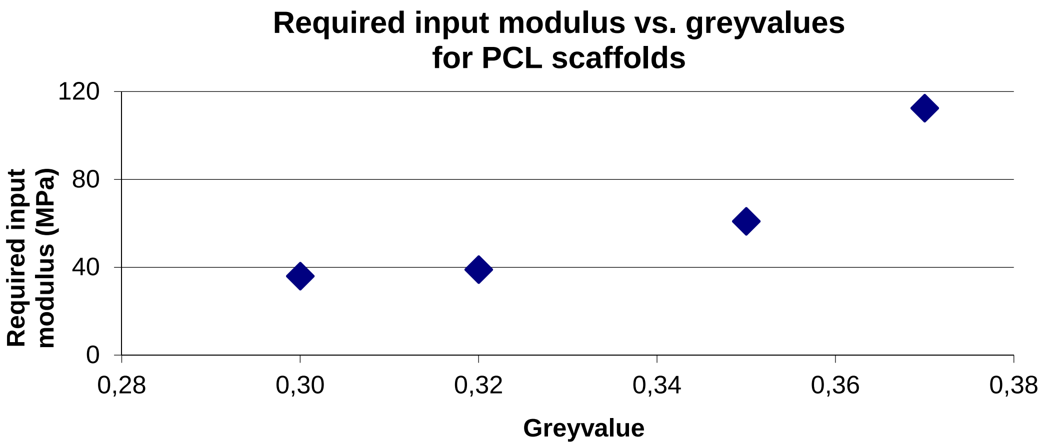

Fig. 5: Required input moduli versus average greyvalue for PCL scaffolds. This graph suggests that higher greyvalues equate with stiffer material properties.

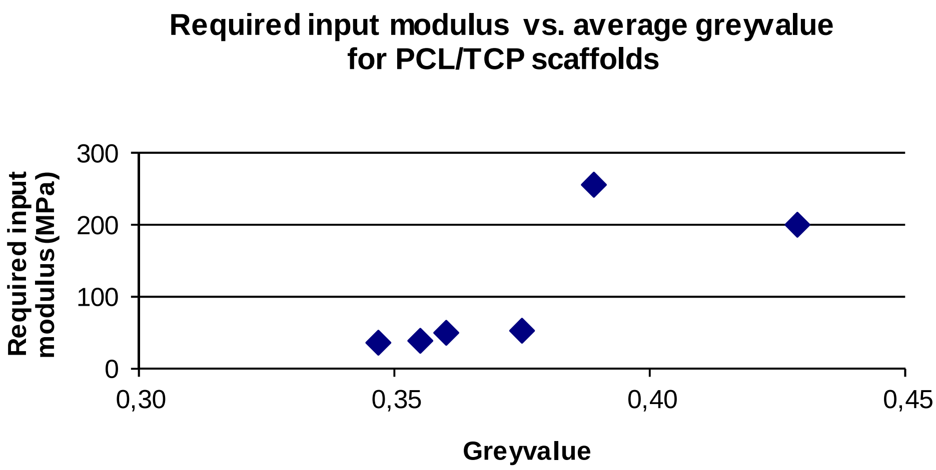

Fig. 6: Required input moduli versus average greyvalue for PCL/TCP scaffolds. This graph suggests that higher greyvalues equate with stiffer material properties.

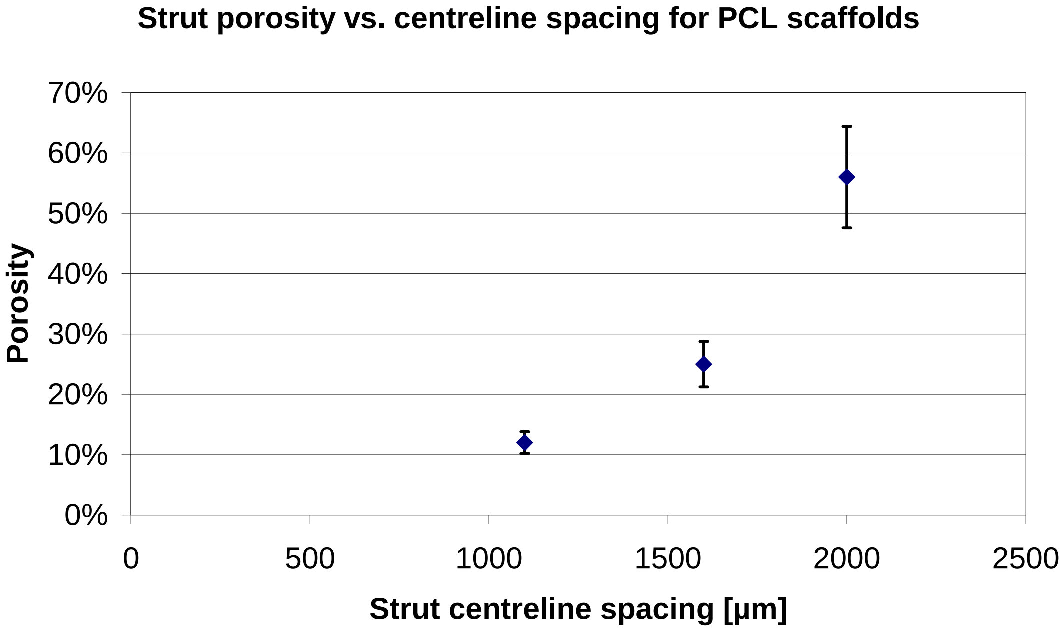

Fig. 7: Strut porosity vs. centreline spacing.

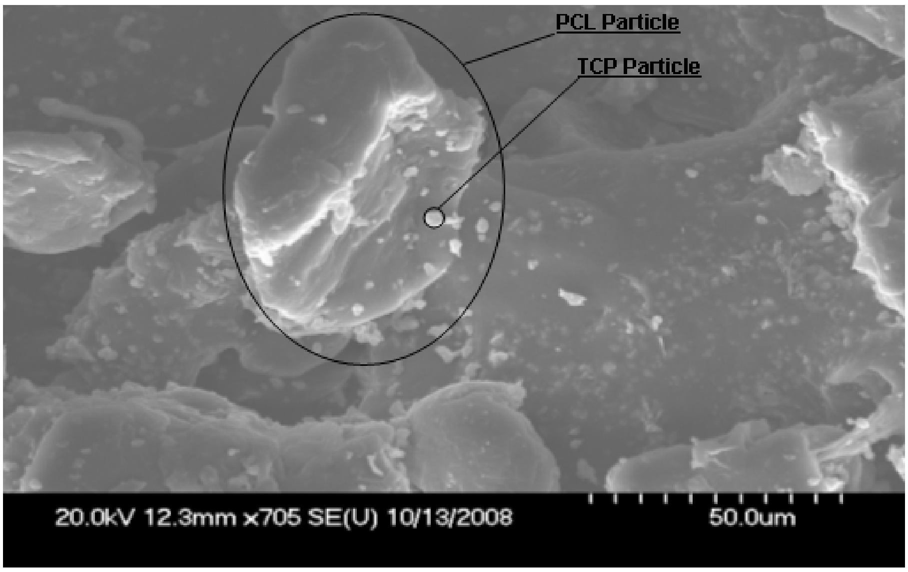

Fig. 8: SEM images of the PCL/TCP scaffolds. The TCP powder particles were much smaller than the PCL powder particles.

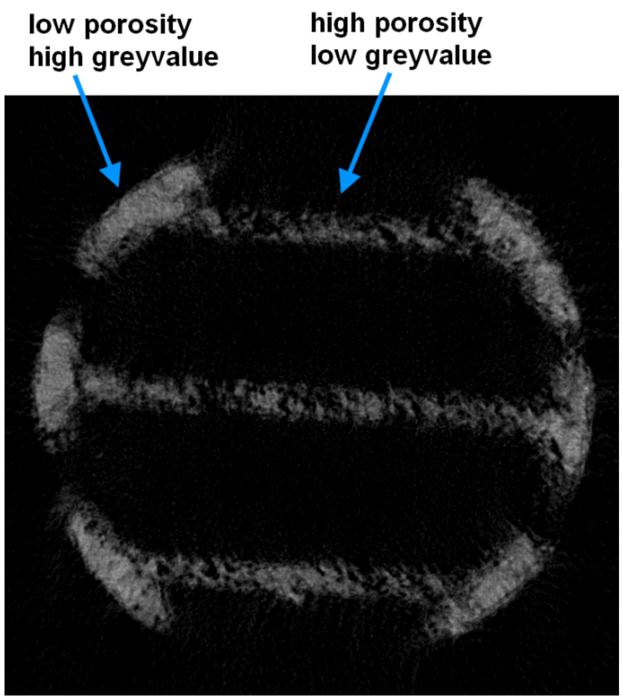

Fig. 9: The area with high greyvalues had lower porosity than the areas with low greyvalues.

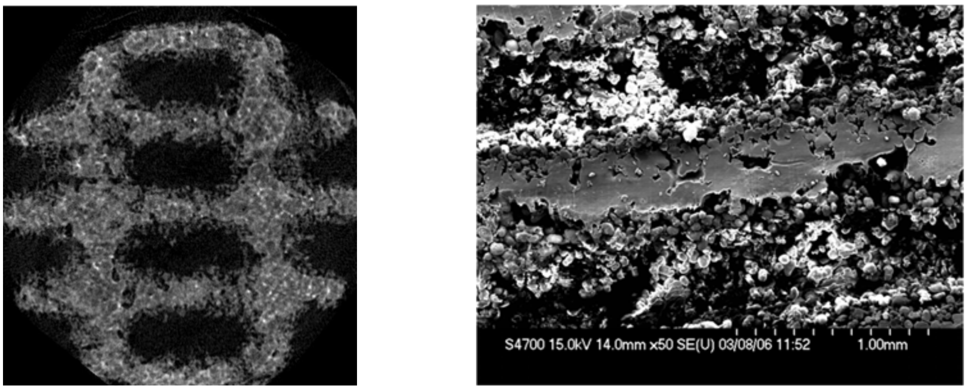

Fig. 10: a) µCT scan images show struts have higher greyvalues along their centrelines than along their edges. b) SEM image shows strut has smooth surface along its centre. This is because the powder particles are fully sintered here. At the edges surface is rough, powder particles are only partially sintered.

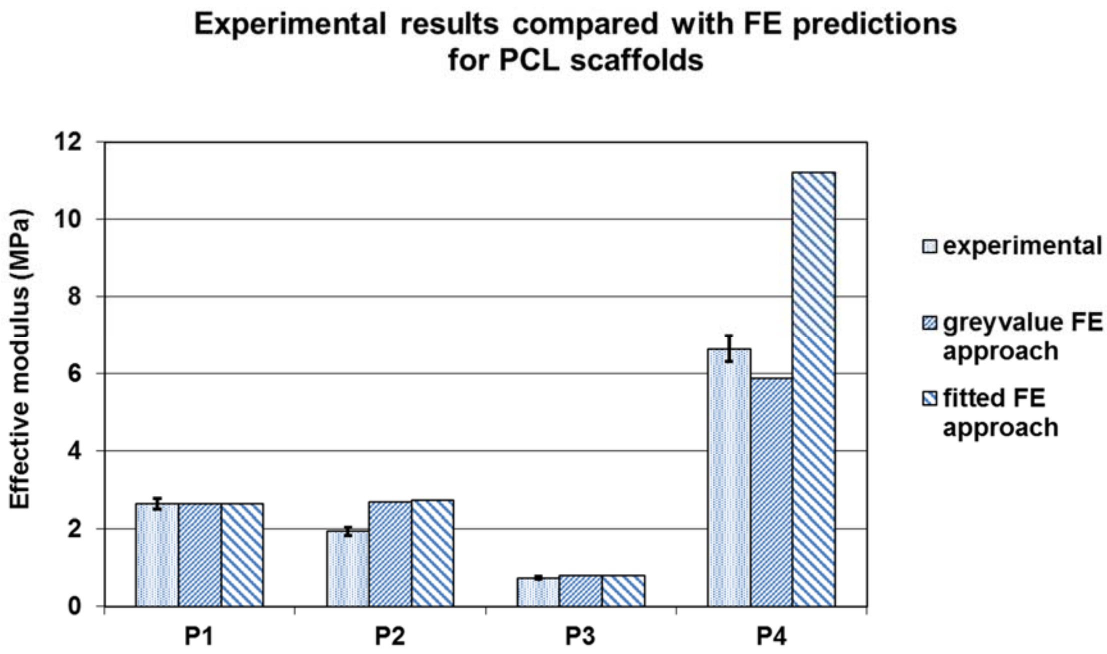

Fig. 11: A comparison of the *greyvalue FE approach* predictions, *fitted FE approach* predictions and experimental results from compression tests for the PCL scaffolds. The *greyvalue FE approach* predictions are closer to the experimental values than the *fitted FE approach* ones. Note: as in Fig. 3, the values for the scaffold P3 are scaled up by an order of magnitude (x10) for visualisation purposes.

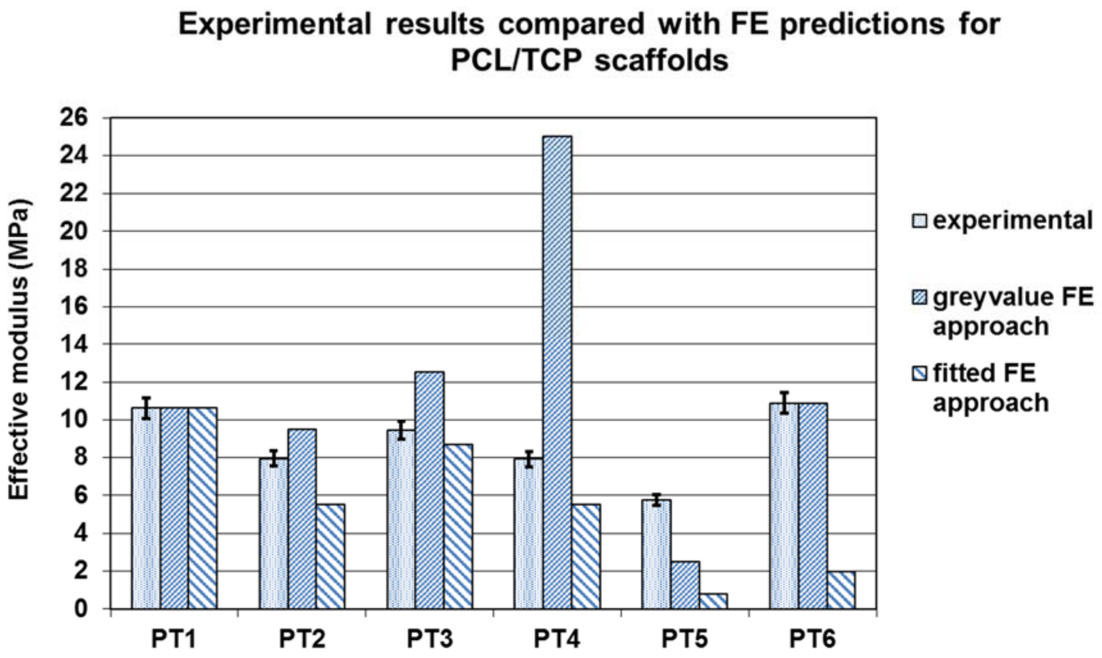

Fig. 12: A comparison of *greyvalue FE approach* predictions, *fitted FE approach* and experimental results from compression tests for the PCL/TCP scaffolds. The *greyvalue FE approach* predictions are less accurate than the *fitted FE approach* predictions.

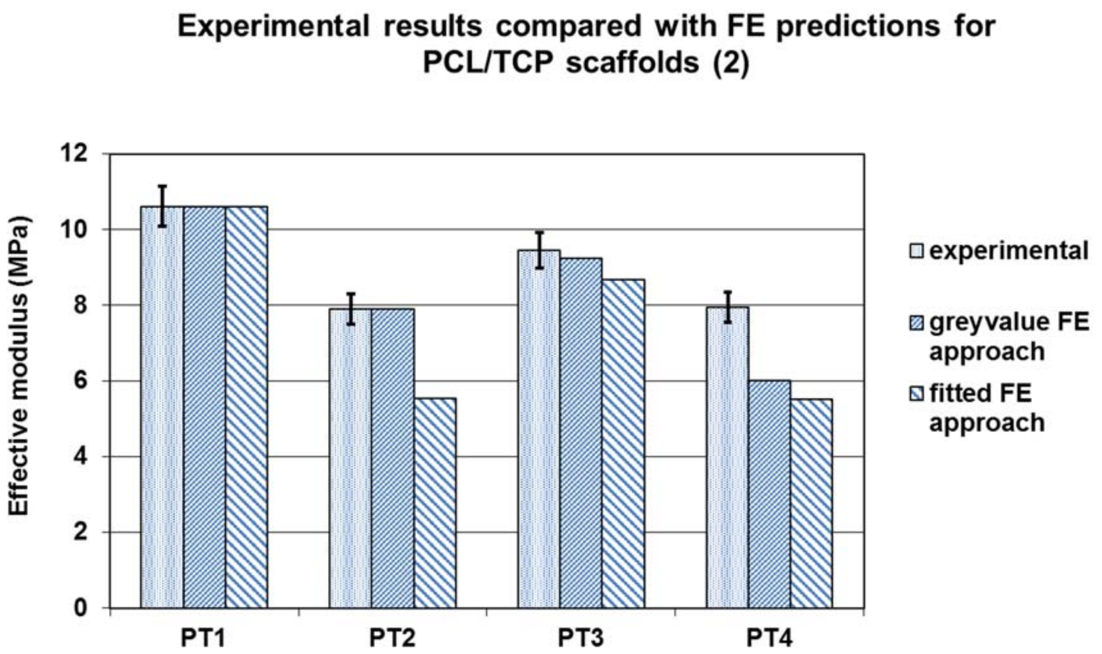

Fig. 13: A comparison of *greyvalue FE approach* predictions, *fitted FE approach* predictions and experimental results from compression tests for the PCL/TCP scaffolds. In this case data from PT5 and PT6 (unit cell based scaffolds) was ignored for the *greyvalue FE approach*, and the *greyvalue FE approach* predictions are closer to the compression test results than the *fitted FE approach* predictions.

a) b)
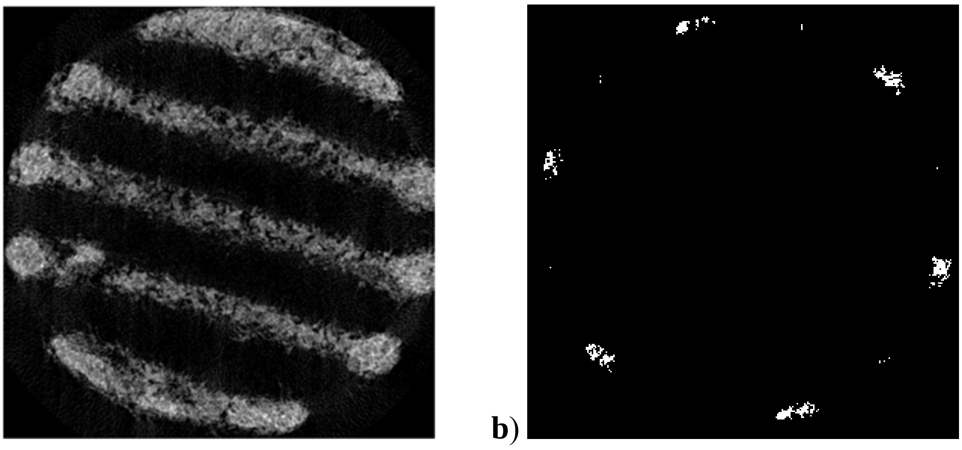

Fig. 14: a) µCT scan image of the P4 scaffold. b) Areas in this scaffold where continuous paths of material ran from top to bottom. The continuous paths are located in the areas of high greyvalues in (a).